THE JOURNAL OF PHYSICAL CHEMISTRY C

Article

Cite This: J. Phys. Chem. C 2018, 122, 13455−13461

pubs.acs.org/JPCC

Synthesis and Photophysical Properties of a Covalently Linked Porphyrin Chromophore−Ru(II) Water Oxidation Catalyst Assembly on SnO_2 Electrodes

Animesh Nayak,[†,§] Ke Hu,[†,§,‡] Subhangi Roy,[§] M. Kyle Brennaman,[§] Bing Shan,[§] Gerald J. Meyer,*[,§] and Thomas J. Meyer*[,§]

[§]Department of Chemistry, University of North Carolina at Chapel Hill, Chapel Hill, North Carolina 27599, United States

[‡]Department of Chemistry, Fudan University, Shanghai 200433, P. R. China

Supporting Information

ABSTRACT: We describe here the preparation and surface photophysical properties of a covalently linked, chromophore-catalyst assembly between a phenyl phosphonate-derivatized pentafluorophenyl-substituted porphyrin and the water oxidation catalyst, $[Ru^{II}(terpyridine)(2\text{-benzimidazolylpyridine})(OH_2)]^{2+}$, in a derivatized assembly of porph-$Ru^{II}-OH_2^{2+}$. The results of nanosecond transient absorption measurements on nanoparticle SnO_2 electrodes in aqueous acetate buffer at pH 4.7 are consistent with rapid electron injection into SnO_2 with transfer of oxidative equivalents to the assembly. Electron transfer from the singlet excited state of the porphyrin to the conduction band of the electrode, $SnO_2(e^-)$|-porph$^+$-$Ru^{II}-OH_2^{2+}$, is favored as the porphyrin singlet excited state lies 0.44 eV above the SnO_2 conduction band edge. Electron injection is rapid ($\langle\tau_{inj}\rangle < 10^{-8}$ s), and occurs with high efficiency. Based on measured redox potentials, following excitation and injection, intra-assembly oxidation of the catalyst, -porph$^+$-$Ru^{II}-OH_2^{2+}$ → -porph-$Ru^{III}-OH^{2+}$ + H^+, is favored in the transient equilibrium state by 0.62 eV at pH 4.7. However, immediately after the flash, a distribution exists at the surface between isomers with $SnO_2(e^-)$|-porph$^+$-$Ru^{II}-OH_2^{2+}$ undergoing back electron transfer to the surface with an average lifetime of $\langle\tau_1\rangle \sim 10^{-7}$ s and a slower component for back electron transfer from $SnO_2(e^-)$|-porph-$Ru^{III}-OH^{2+}$ with $\langle\tau_2\rangle \sim 4 \times 10^{-5}$ s.

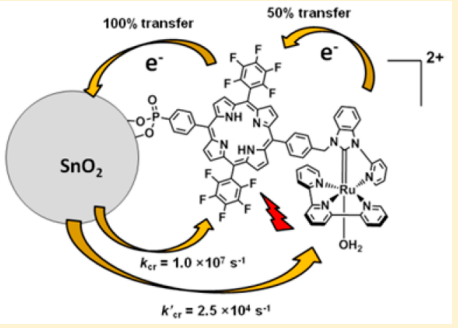

INTRODUCTION

In dye-sensitized photoelectrosynthesis cells (DSPECs) for water oxidation,[1] the chromophore absorbs light and injects electrons into an n-type semiconductor oxide, typically TiO_2 or SnO_2, transferring oxidative equivalents to a catalyst for H_2O oxidation.[2,3] Porphyrins are appealing as chromophores because of their high visible molar absorptivities and the ability to use chemical synthesis to modify electronic properties systematically by making substituent changes.[4,5] A significant number of porphyrin-based chromophore−catalyst assemblies have been reported which undergo light absorption, charge injection on semiconductor metal oxides, and transfer of an oxidative equivalent for H_2O oxidation catalysis.[6−8] However, little is known about interfacial electron transfer dynamics in these assemblies that is crucial to improving the overall efficiency in a DSPEC configuration.[3]

We report here the synthesis and photophysical characterization of the covalently linked chromophore−catalyst assembly between a pentafluorophenyl-substituted porphyrin, 5,15-pentafluorophenyl-10-(4-phosphonatophenyl)-20-phenyl porphyrin, as a chromophore and a derivative of the known water oxidation catalyst, $[Ru(tpy)(bim\text{-}py)(OH_2)]^{2+}$ (tpy is 2,2′:6′,2″-terpyridine; bim-py is 1-methyl-3,1′-pyridyl benzimidazole) (Figure 1). The choice of the assembly and its design was based on the well-established mechanistic chemistry of the catalyst in solutions, on surfaces, and in molecular assemblies as well as on the spectroscopic and electrochemical properties of the porphyrin with the goal of developing assemblies for light-driven water oxidation.[7,9,10]

On the basis of previous electrochemical measurements, the Ru(II) form of the catalyst undergoes a series of pH-dependent oxidations based on the $Ru^{III}{=}OH^{2+}/Ru^{II}-OH_2^{2+}$ and $Ru^{IV}-O^{2+}/Ru^{III}-OH^{2+}$ couples with further oxidation and proton loss leading to $Ru^{V}{=}O^{3+}$ which is the key intermediate in water cycles.[9] The perfluoroporphyrin was of interest because of the light absorptivity characteristics of the porphyrin and its ground and excited state energetics. Based on previous studies, the excited state potential of the pentafluorophenyl-substituted porphyrin is −0.44 V vs NHE, which is sufficiently negative to ensure efficient excited state injection into the conduction band of SnO_2.[7,10] It also has an electrochemical potential for the first

Special Issue: Prashant V. Kamat Festschrift

Received: November 28, 2017
Revised: January 10, 2018
Published: January 11, 2018

DOI: 10.1021/acs.jpcc.7b11711
J. Phys. Chem. C 2018, 122, 13455−13461

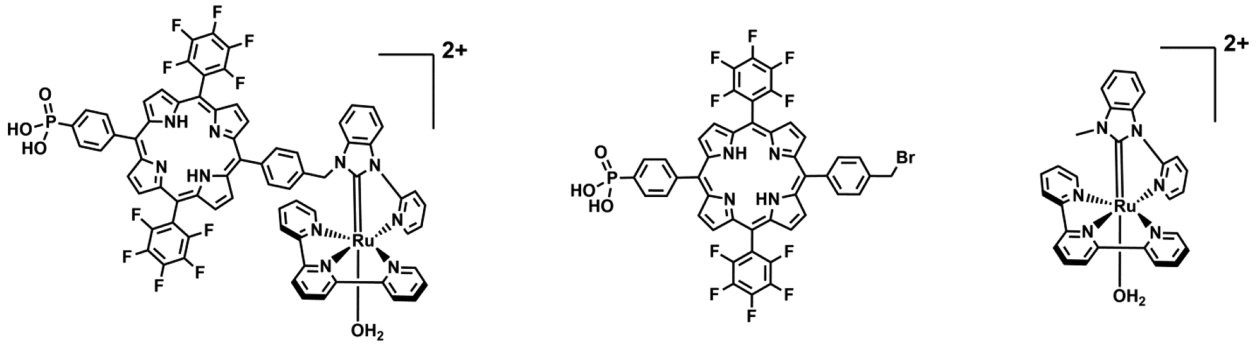

Figure 1. Molecular structures of the chromophore−catalyst assembly (**1**), model chromophore (**2**), and the catalyst (**3**) used in this study.

oxidation at 1.54 V vs NHE which is sufficiently positive to oxidize the catalyst to $Ru^{V}{=}O^{3+}$ (Scheme 1).[7,10]

Scheme 1. Energy Level Diagram Showing the Relevant Levels for Electron Injection from the Excited Chromophore and Different Electron Transfer Processes

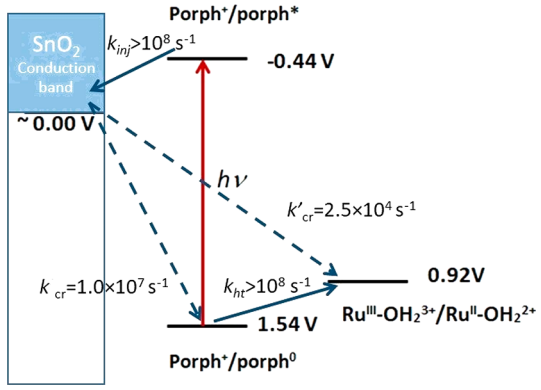

The use of a bridging ligand in the assembly, as a way of connecting chromophore and catalyst and controlling the local environment, offers significant advantages. First, it provides the simplicity of one-step sensitization on the electrode. Second, the covalent bond plays an important role in providing a stable link between the chromophore and the catalyst, creating a dual function assembly. Third, the covalent linkage strategy provides a basis for controlling the relative structural orientation of the catalyst relative to the surface with the catalyst away from the surface and, depending on the nature of molecular bridges, of slowing back electron transfer from the surface following injection.[11]

Here we describe the results of nanosecond pump−probe laser flash photolysis experiments on the phosphonate-derivatized assembly termed porph-$Ru^{II}{-}OH_2^{2+}$ (**1**, Figure 1) anchored to mesoporous nanocrystalline SnO_2 thin films in an aqueous acetate buffer at pH 4.7. In any water oxidation scheme based on chromophore−catalyst assemblies of this kind, the chromophore−catalyst structure is ultimately responsible for the absorption of 4 photons and their interaction with the assembly and interface in driving the $4e^{-}/4H^{+}$ oxidation of water in multiple cycles. The goal here was to explore the first stage of the process by using single-photon transient absorption measurements.

EXPERIMENTAL SECTION

Synthesis. All reagents and solvents were obtained from either Sigma-Aldrich or Fisher Scientific and used without any purification. Inert atmosphere manipulations were carried out under N_2 prepurified by passage through a drying tower (Linde 3 Å molecular sieves). Deuterated solvents $CDCl_3$ and DMSO-d_6 for NMR were obtained from Cambridge Isotope Laboratories Inc. Compounds **4**,[12] **5**,[13] **6**,[14] **7**,[10] **8**,[15] and **10** were synthesized following procedures published earlier. The transient absorption apparatus was described elsewhere.[1] Metal oxide electrodes were prepared following published procedures.[16,17]

*5-(Ph-CH_2-bim-py)-10,20-bis(PhF_5)-15-(PhPO_3Et_2) Porphyrin (**9**).* Compound **7** (120 mg, 0.12 mmol) was refluxed with of excess of compound **8** (354 mg, 1.76 mmol) in toluene (3 mL) with continuous stirring. After 16 h, the reaction mixture was cooled to room temperature, and solvent was removed. The crude product was purified by silica gel column chromatography using a CH_2Cl_2/MeOH mixture with gradual increase of MeOH from 2% to 10%. The major reddish purple band was collected. Solvent was removed to get the desired product as a red solid compound (110 mg, yield = 77% based on compound **7**). ^{1}H NMR (400 MHz, $CDCl_3$): 12.90 (s, 1H), 8.75−8.90 (m, 10H), 8.72 (dd, J = 8 Hz, J = 4 Hz, 1H), 8.28−8.33 (m, 2H), 8.16−8.26 (m, 5H), 8.04 (d, J = 8 Hz, 2H), 7.98 (m, 1H), 7.81 (m, 2H), 7.56 (dd, J = 8 Hz, J = 4 Hz, 1H), 6.50 (s, 2H), 4.38 (m, 4H), 1.51 (t, J = 8 Hz, 6H), −2.92 (s, 2H).

*Ru(II)(terpy)(bim-py-5-(CH_2Ph)-10,20-bis(PhF_5)-15-(PhPO_3Et_2) porphyrin)Cl_2 (**11**).* Compound **10** (50 mg, 0.04 mmol) and $[Ru(tpy)Cl_2]_2$ (33.2 mg, 0.04 mmol) were added to a Teflon microwave vessel, and EtOH/H_2O (2:1, 20 mL) mixture was added. The mixture was then heated in the microwave at 165 °C for 20 min. After cooling, the reaction mixture was filtered and washed with 5 mL of EtOH/H_2O (2:1) mixture. Filtrate was collected, and solvent was removed. The crude product was purified by Sephadex (LH-20) column chromatography using $CHCl_3$/MeOH (1:1) as eluent. The first dark red band was collected, and solvent was removed to get a dark red solid (45 mg, yield = 72% based on compound **10**). ^{1}H NMR (400 MHz, $CDCl_3$): 10.42 (d, J = 4 Hz, 1H), 8.92 (d, J = 8 Hz, 4H), 8.85 (t, J = 4 Hz, 4H), 8.62−8.74 (m, 3H), 8.48 (d, J = 8 Hz, 2H), 8.41 (t, J = 8 Hz, 1H), 8.31−8.37 (m, 3H), 8.22−8.30 (m, 3H), 7.74−7.82 (m, 4H), 7.71 (t, J = 4 Hz, 1H), 7.53 (t, J = 8 Hz, 1H), 7.38−7.47 (m, 2H), 7.24 (t, J = 8 Hz, 2H), 6.72 (d, J = 8 Hz, 2H), 5.23 (s, 2H), 4.34−4.50 (m, 4H), 1.56 (t, J = 8 Hz, 6H), −2.88 (s, 2H). ^{19}F NMR (376 MHz, $CDCl_3$): −136.82 (dd, 4F), −151.74 (t, 2F), −161.57 (td, 4F). ^{31}P NMR (162 MHz, $CDCl_3$): 18.56 (s).

DOI: 10.1021/acs.jpcc.7b11711
J. Phys. Chem. C 2018, 122, 13455−13461

Scheme 2. Synthetic Scheme for Chromophore−Catalyst Assembly 1

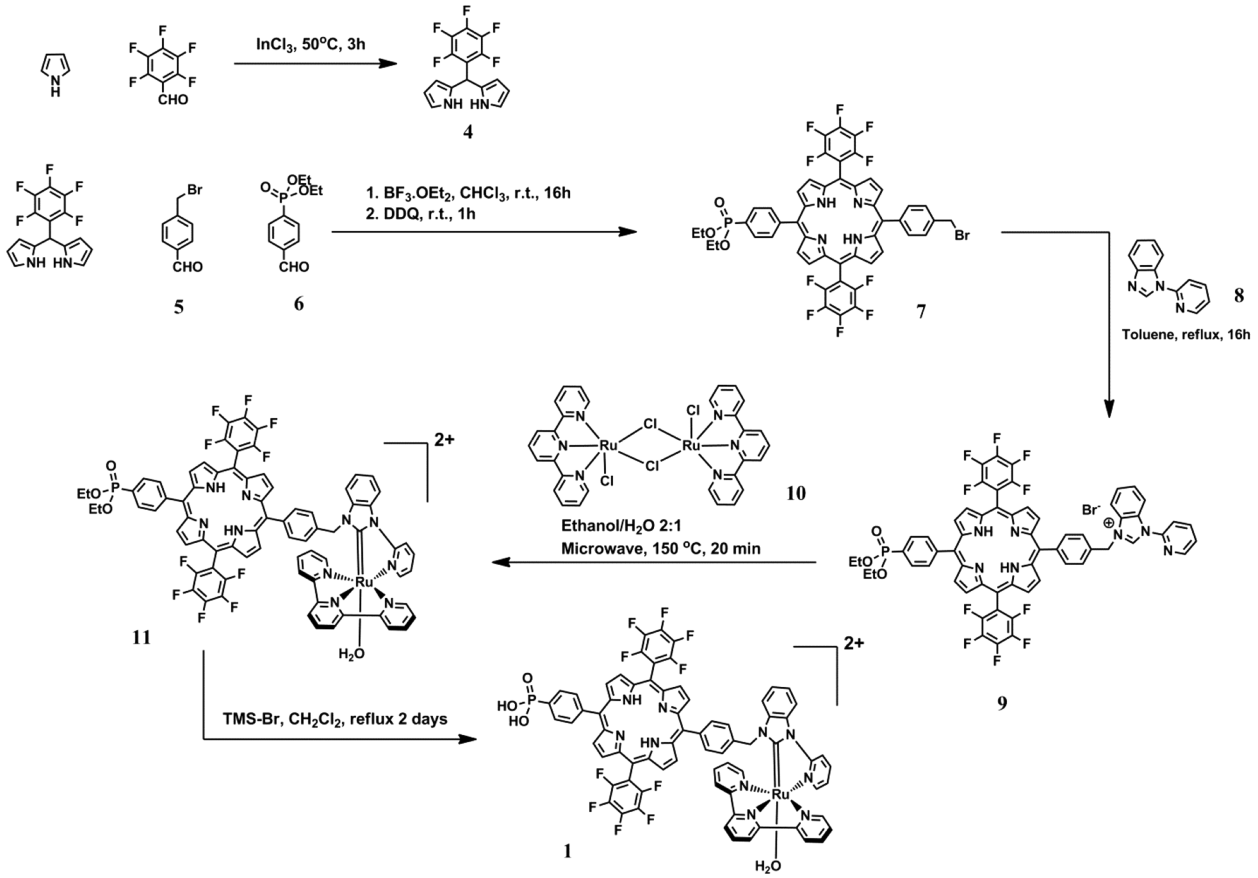

*Ru(II)(terpy)(bim-py-5-(CH_2Ph)-10,20-bis(PhF_5)-15-($PhPO_3H_2$) porphyrin)Cl_2 (**1**).* Compound **11** (40 mg, 25 μmol) was dissolved in anhydrous CH_2Cl_2 (5 mL). Bromotrimethylsilane (30 μL, 0.23 mmol) was added, and the mixture was refluxed under N_2 for 2 days. After cooling, the solvent was removed, and the product was stirred in H_2O (10 mL) for 3 h. The solid was filtered and washed with H_2O. The crude material was purified by Sephadex (LH-20) column chromatography using $CHCl_3$/MeOH (1:1) as eluent. A major dark red band was collected, and solvent was removed to obtain dark red solid (34 mg, yield = 90% based on compound **11**). ^{1}H NMR (400 MHz, DMSO-d_6): 10.29 (d, J = 4 Hz, 1H), 9.34 (d, J = 4 Hz, 2H), 9.27 (d, J = 4 Hz, 2H), 8.92 (d, J = 4 Hz, 2H), 8.77−8.89 (m, 5H), 8.69 (d, J = 8 Hz, 2H), 8.58 (d, J = 8 Hz, 1H), 8.43 (t, J = 8 Hz, 1H), 8.30−8.39 (m, 3H), 8.11−8.19 (m, 2H), 8.04 (t, J = 8 Hz, 2H), 7.77−7.86 (m, 3H), 7.71 (d, J = 4 Hz, 2H), 7.50 (t, J = 4 Hz, 1H), 7.36−7.45 (m, 4H), 6.59 (d, J = 8 Hz, 2H), 5.08 (s, 2H), −3.09 (s, 2H). ^{19}F NMR (376 MHz, $CDCl_3$): −139.35 (dd, 4F), −153.65 (t, 2F), −162.65 (td, 4F). ^{31}P NMR (162 MHz, $CDCl_3$): 12.43 (t). ESI-MS (FT-ICR): m/z = 708.098 (Calculated 708.099 for [compound **1** − H_2O]$^{2+}$).

Metal Oxide Thin-Film Preparation. Mesoporous nanocrystalline SnO_2 or ZrO_2 colloidal pastes were prepared as previously described.[18] The pastes were doctor bladed onto 1 mm thick microscopic glass slides using Scotch tape as the spacer and sintered under air at 450 °C for 30 min. The slides were then immersed in dye loading solution (MeOH/CH_2Cl_2 1:1) overnight. The apparent surface coverage (Γ) was calculated using equation $\Gamma = A/(1000 \times \varepsilon)$, where A and ε are absorbance and absorptivity at a particular absorption wavelength.

Spectroscopy. Ground state absorption measurements were performed on a Cary 50 spectrophotometer. Nanosecond transient absorption measurements were carried out on an Edinburgh LP920 laser flash photolysis spectrometer equipped with a Spectra-Physics Quanta-Ray Lab-170 Nd:YAG laser combined with a VersaScan OPO, which has been previously described in detail.[19] Briefly, the pulsed laser was directed 45° to the surface of the sensitized substrate that was diagonally positioned in a 1 cm path length cuvette. A 450 W Xe arc lamp served as the probe light. Detection was achieved by a photomultiplier tube (Hamamatsu R928) coupled to a monochromator. Signal averaging of 25−75 laser shots was used to achieve satisfactory S/N.

Data Analysis. Global analysis of the transient absorption spectra was performed using a customized code written in Mathematica 10. Briefly, kinetic data at multiple wavelengths with best signal-to-noise ratio were fit to a sum of two stretched exponential functions: $\Delta A(\lambda,t) = A_{\text{Porph}^+}(\lambda)e^{-(k_{\text{porph}^+}t)^{\beta}} + A_{\text{Ru}^{\text{III}}}(\lambda)e^{-(k_{\text{Ru}^{\text{III}}}t)^{\beta}}$, where A_{Porph^+} and $A_{\text{Ru}^{\text{III}}}$ are wavelength-dependent transient absorbance for one electron oxidized porphyrin and one electron oxidized ruthenium carbene catalyst; k_{Porph^+} and $k_{\text{Ru}^{\text{III}}}$ are the characteristic rate constants, respectively; and β is inversely related to the breadth of an underlying Lévy distribution of rate constants. k_{Porph^+}, $k_{\text{Ru}^{\text{III}}}$, and β values were averaged from the fits and substituted into the double stretched exponential function. The function was then used to fit all of the wavelength kinetics to obtain the preexponential factors. The time-dependent concentration changes were obtained by a least-squares minimization routine.

DOI: 10.1021/acs.jpcc.7b11711
J. Phys. Chem. C 2018, 122, 13455−13461

RESULTS AND DISCUSSION

Design and Synthesis of the Assembly. As shown by the structure in Figure 1, the porphyrin−Ru(II) polypyridyl assembly features a pentafluorophenyl-substituted porphyrin with a high potential porph$^{+/0}$ couple as the chromophore and a [Ru(tpy)(bim-py)(OH$_2$)]$^{2+}$ catalyst derivative linked by a methylene spacer. Electron-withdrawing pentafluorophenyl substituents were added as substituents to increase $E^{o\prime}$ for the first porphyrin oxidation, $E_1{}^{o\prime}$(porph$^{+/0}$), to a value sufficiently positive to drive water oxidation by the covalently linked catalyst. The porphyrin was also phenylphosphonate-derivatized for binding to metal oxide surfaces by formation of the relatively stable aqueous phosphonate-oxide surface binding, a well-established surface-linking motif.[20]

The synthetic methodology for the assembly is shown in Scheme 2. In brief, the porphyrin chromophore was first synthesized by acid-catalyzed condensation of 5-pentafluorophenyl dipyrroylmethane, 4-phosphonato benzaldehyde, and 4-bromomethyl benzaldehyde to give porphyrin **7**. In turn, porphyrin **7** was allowed to react with the 2-benzimidazolyl pyridine (bim-py) ligand to form derivatized porphyrin-(bim-py). Finally, the assembly was prepared by the complexation reaction between the porphyrin-(bim-py) and the Ru(II) precursor complex (Ru(II)(tpy)Cl$_2$)$_2$. The phosphonate group of the assembly was subsequently hydrolyzed by reaction with bromotrimethylsilane followed by treatment with water.

Optical and Electrochemical Properties. The ground state absorption spectra of the assembly, the porphyrin, and the catalyst in solution are shown in Figure 2. In the assembly, there

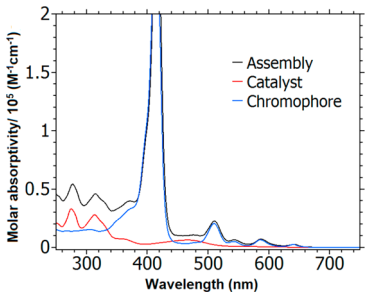

Figure 2. Ground-state UV−vis absorption spectra of the chromophore (blue), catalyst (red), and assembly **1** (black) in solution in MeOH/CH$_2$Cl$_2$ (1/1) (blue and black lines) and MeOH (red line).

was very little electronic coupling between the porphyrin chromophore and Ru(II) catalyst, as evident from spectral comparisons with a summation of absorption spectra of porphyrin and catalyst matching well with the absorption spectrum of assembly **1**. The spectrum features absorptions in the UV region due to terpyridine-based $\pi-\pi^*$ transitions. The visible region includes an absorption at ∼400 nm with high absorptivity, the Soret band of the porphyrin, and absorptions around 450−700 nm arising from porphyrin Q bands. For the assembly, absorption in the visible is largely dominated by the porphyrin with the catalyst-based MLCT transitions of lower absorptivity.

The first ground state porphyrin reduction potential was at $E^{o\prime}$ = 1.54 V vs NHE in CH$_2$Cl$_2$ at room temperature, and the excited state reduction potential for the porph$^{+/}$* couple was estimated as −0.44 V vs NHE by subtracting E_{0-0} (1.9 eV) from the ground state potential.[10] The excited state potential for the porph$^{+/}$* couple is sufficiently reducing for electron injection into SnO$_2$ with a conduction band potential of E_{cb} = 0.0 V under the same conditions (Scheme 1).[7,10] The properties of the catalyst, [Ru(tpy)(bim-py)(OH$_2$)]$^{2+}$, toward water oxidation were reported earlier.[9] At pH 4.7, its catalytic cycle involves sequential 1e$^-$/1H$^+$ oxidation to Ru^{III}−OH^{2+} and Ru^{IV}=O^{2+} followed by further oxidation of Ru^{IV}=O^{2+} to Ru^{V}(O)$^{3+}$ with water attack to give an intermediate peroxide, Ru^{III}−OOH^{2+}. The peroxide undergoes further oxidation and O$_2$ loss and re-enters the catalytic cycle.[9]

Cyclic voltammetry of the assembly on nano ITO surfaces was performed in CH$_2$Cl$_2$ with 0.1 M tetra-*n*-butylammonium hexafluorophosphate as electrolyte. The cyclic voltammograms under these conditions included waves for the Ru$^{3+/2+}$ couple of the catalyst at 0.95 V, a wave for the Ru$^{4+/3+}$ couple at 1.29 V, and a wave for the porph$^{+/0}$ couple at ∼1.54 V vs NHE (Figure S1). From the known electrochemistry of the catalyst, [Ru^{II}(tpy)-(bim-py)(OH$_2$)]$^{2+}$, and its pH dependence, pK_a = 4.5 for Ru^{III}−OH$_2{}^{3+}$.[21]

Photoinduced Charge Separation. Interfacial electron transfer dynamics were investigated for the assembly of **1** and the porphyrin loaded onto nanocrystalline SnO$_2$ films on FTO (fluorine-doped SnO$_2$) coated glass slides (4 μm thick films, ∼15 nm in diameter particles), to give SnO$_2$|-porph-Ru^{II}−OH$_2{}^{2+}$ and SnO$_2$|-porph. Nanosecond transient absorption measurements were carried out in aqueous media (pH 4.7, 0.1 M acetate buffer, with 0.4 M added LiClO$_4$) for both the porphyrin and the assembly. Porphyrin and assembly were loaded onto the mesoporous films by soaking in solutions of assembly **1** or the porphyrin (both ∼8 × 10^{-5} M, as calculated from the absorbance of the electrodes) in MeOH/CH$_2$Cl$_2$ (1:1) overnight (Figure S2).

In a previous study from our group, it was observed that a structurally similar bispentafluorophenyl-substituted porphyrin shows emission quenching when immobilized on SnO$_2$, consistent with electron injection from the porphyrin excited state into the SnO$_2$ conduction band.[7] This observation was the basis for using SnO$_2$ as the semiconductor metal oxide for this study. In a first series of experiments, transient absorption spectral features and time dependences were compared for the porphyrin triplet and porphyrin cation radical by transient absorption measurements (λ_{ex} = 425 nm) on the inert oxide ZrO$_2$, ZrO$_2$|-porph, and on SnO$_2$, SnO$_2$|-porph (Figure S3) in pH 4.7 acetate buffer at 25 °C. Electron injection into ZrO$_2$ does not occur because of its highly negative potential for conduction band.[1] On ZrO$_2$, at the first observation time of 30 ns, characteristic absorption features for the porphyrin triplet excited state appear in the transient difference spectra.[22]

Electron injection is thermodynamically favorable on SnO$_2$, and transient difference spectra include the characteristic feature of the porphyrin radical cation, SnO$_2$|-porph$^{+\bullet}$. Comparison of transient difference spectra for ZrO$_2$|-porph and SnO$_2$|-porph shows that transient absorption features for the porphyrin radical cation and porphyrin triplet state are very similar, as found for other porphyrins.[7,23] However, subtle differences between the transient radical cation and triplet state do exist. They include a low absorptivity bleach feature at ∼550 nm and enhanced absorptivity in the 600−800 nm region for the excited SnO$_2$|-porph consistent with the appearance of the porphyrin cation radical.

Triplet state decay of the porphyrin on ZrO$_2$ was nonexponential, (Figure S4) but could be fit to the stretched exponential function in eq 1[24,25] with an average rate constant of 1.5 (±0.2) × 10^3 s^{-1}. The average rate constants were calculated

DOI: 10.1021/acs.jpcc.7b11711
J. Phys. Chem. C 2018, 122, 13455−13461

from the first moment of the Lévy distribution function used to fit the data in eq 2. The standard error was estimated from fitting of multiple kinetic data over at least three different wavelengths as was done throughout. The extended lifetime for the triplet on ZrO_2 was not observed for SnO_2|-porph for which the loss of transient occurred with an average rate constant, $\bar{k}$ (eq 2), of 1.9 ($\pm$0.2) $\times$ 10^5 s^{-1} (Figure S4). The absence of this long-lived component is consistent with injection into SnO_2 by the porphyrin singlet excited state.

$$\Delta A = Ae^{-(kt)^{\beta}} \tag{1}$$

$$\bar{k} = \left[\frac{1}{k\beta} \times \Gamma\left(\frac{1}{\beta}\right)\right]^{-1} \tag{2}$$

Nanosecond transient absorption difference spectra for the assembly anchored as SnO_2|-porph-Ru^{II}−OH_2^{2+}, in pH 4.7 acetate buffer after 425 nm laser excitation with time delays of 30 ns to 18 μs, are shown in Figure 3(A). One significant feature that

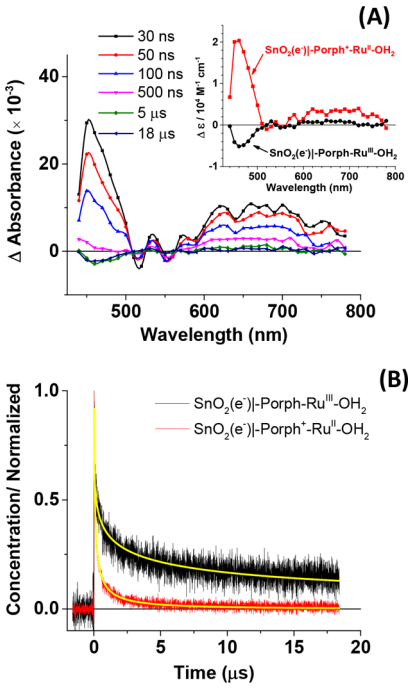

Figure 3. Time-resolved spectroscopic characterization of photo-induced interfacial charge recombination kinetics for the SnO_2|-**1** electrode (A) Transient absorption difference spectra on SnO_2 at pH = 4.7 in a 0.1 M acetate buffer solution after 425 nm laser excitation. The inset shows decay associated spectra that illustrate the transient appearance of two distinct charge separated states. (B) Deconvoluted, normalized concentration changes for $SnO_2(e^-)$|-Porph$^{+\bullet}$-Ru^{II}-OH_2 (red) and $SnO_2(e^-)$|-Porph-Ru^{III}-OH_2 (black), as a function of time.

differs notably from the SnO_2|-porph spectrum is that the spectra are no longer normalizable at different time delays, consistent with more than one transient intermediate on the surface. The bleach centered at ~460 nm after a 5 μs time delay was significantly different from that for SnO_2|-porph. The loss of the oxidized porphyrin absorption features and the appearance of the absorption bleach are both consistent with intra-assembly oxidation of the ruthenium carbene catalyst by the oxidized porphyrin following injection. An excitation/electron transfer mechanism is shown in eqs 3−5. Because of the small spectral features for the Ru(III) form of the catalyst, it was not possible to discern the protonation state for Ru(III), and eq 5 is written showing the aqua form of the complex. Given the pK_a for −$RuOH_2^{3+}$, both forms could be present in solution.

$$SnO_2\text{|-Porph-}Ru^{II}-OH_2^{2+} \xrightarrow{h\nu} SnO_2\text{ |-}^1\text{ Porph*-}Ru^{II}-OH_2^{2+} \tag{3}$$

$$SnO_2\text{ |-}^1\text{ Porph*-}Ru^{II}-OH_2^{2+} \xrightarrow{k_{inj}} SnO_2(e^-)\text{|-Porph}^{+\cdot}\text{-}Ru^{II}-OH_2^{2+} \tag{4}$$

$$SnO_2(e^-)\text{|-Porph}^{+\cdot}\text{-}Ru^{II}-OH_2^{2+} \xrightarrow{k_{ht}} SnO_2(e^-)\text{|-Porph-}Ru^{III}-OH_2^{3+} \tag{5}$$

As noted above, the kinetic overlap between the oxidized porphyrin and the catalyst complicate the interpretation of the transient spectra. Application of global analysis results in decay elements for the decay-associated spectra (DAS) from two contributors.[11,26] Application of the kinetic fitting procedure with components from SnO_2 (e^-)|-Porph$^{+\bullet}$-Ru^{II}−OH_2^{3+} and SnO_2 (e^-)|-Porph-Ru^{III}−OH_2^{3+}, as a function of time, were derived by spectral deconvolution. Analysis of the data with global analysis shows that following 425 nm excitation the state, SnO_2 (e^-)|-Porph-Ru^{III}−OH_2^{3+}, is formed initially and reaches its maximum concentration of 3.3 nmol/cm^2 immediately after the laser pulse. Given the ~10 ns time scale for the laser pulse, these observations are consistent with ultrafast chromophore excited state injection with $k_{inj} > 10^8$ s^{-1}, followed by rapid hole transfer (k_{ht}) (eq 5), with $k_{ht} > 10^8$ s^{-1}.

Also consistent with the transient results is the appearance of the porphyrin-trapped charge-separated state, SnO_2 (e^-)|-Porph$^{+\bullet}$-Ru^{II}−OH_2, on the surface following excitation. Based on the transient absorption results, the bridge-based state is present after the laser flash at an initial concentration of 2.5 nmol/cm^2 with a relative intramolecular electron transfer quantum yield of 57%.

The appearance of the bridge-based state was unexpected compared to results obtained earlier for related assemblies.[27,28] Based on the electrochemical results, oxidation of the ruthenium carbene catalyst at pH 4.7 occurs at 0.92 V versus NHE, 0.62 V below the potential for porphyrin oxidation.[21] The transient data show that excitation and injection by the assembly is followed by intra-assembly electron transfer to give $SnO_2(e^-)$|-Porph-Ru^{III}−OH^{2+}, but only on about half of the assemblies.

The surface redox-trapping effect observed here for the assembly is a transient phenomenon as shown by the electrochemical results cited above. The origin of the transient effect is not clear. It most probably arises from the non-equilibrium ionic strength conditions at the interface following injection by the porphyrin. The redox-trapping effect was observed even when the assembly was partially loaded on SnO_2 with ~25% of full coverage. Based on spectroscopic observations, we assume that on the surface, on the sub ms time scale, there is a distribution of states at the surface. In approximately half of the surface states, injection is followed by intra-assembly electron transfer to give the completely oxidized assembly. In another fraction of sites, $SnO_2(e^-)$|-Porph$^{+\bullet}$-Ru^{II}−OH_2^{2+} is transiently stabilized on the surface by local medium and ionic strength effects, in part dictated by relatively slow dielectric reorientation near the porphyrin surface.[29,30] Prior research on porphyrin-antenna-type assemblies showed that large driving force for

DOI: 10.1021/acs.jpcc.7b11711
J. Phys. Chem. C 2018, 122, 13455−13461

electron transfer was not a determining factor for quantitative electron transfer.[31] A related observation has been made for the assembly of $[((PO_3H_2)_2bpy)_2Ru(bpy\text{-}bimpy)Ru(tpy)(OH_2)](Cl)_4$ where following oxidation to the mixed valence form, $TiO_2(e^-)$-$[Ru_a^{II}*\text{-}Ru_b^{III}-OH_2]^{5+}$, the excited electron is trapped at the surface-bound chromophore.[32]

Back Electron Transfer. Back electron transfer limits the efficiency of DSPEC devices,[17] and a variety of approaches have been used to minimize the effect. The latter include variations in pH, distance,[21,28] and semiconductor core−shell structure.[16,17] Given the apparent role of medium effects observed here for the same assembly, it was possible to track the impact of distance on electron transfer within the same assembly but from two different acceptors—from the electrode to −Ru(III) and from the electrode to oxidized porphyrin.[26] Kinetic fits to the stretched exponential model in eqs 1 and 2 gave for the adjacent electron transfer reaction $k_{cr} = 1.0\ (\pm 0.3) \times 10^7\ s^{-1}$. Analysis of the data for the slow, remote process gave $k'_{cr} = 2.5\ (\pm 0.4) \times 10^4\ s^{-1}$.

$$SnO_2(e^-)|\text{-}Porph^{+\cdot}\text{-}Ru^{II}-OH_2^{2+} \xrightarrow{k_{cr}} SnO_2|\text{-}Porph\text{-}Ru^{II}-OH_2^{2+} \quad (6)$$

$$SnO_2(e^-)|\text{-}Porph\text{-}Ru^{III}-OH_2^{3+} \xrightarrow{k'_{cr}} SnO_2|\text{-}Porph\text{-}Ru^{II}-OH_2^{2+} \quad (7)$$

The data show that back electron transfer to the remote oxidized carbene catalyst is more than 2 orders of magnitude slower than back electron transfer to the singly oxidized porphyrin. The difference in rate constants is a consequence of the enhanced distance for electron transfer from the Ru(III) acceptor to the electrode, ∼18 Å for $SnO_2(e^-)|\text{-}Porph\text{-}Ru^{III}-OH^{2+}$ and ∼10 Å from the center of the porphyrin ring to the electrode in $SnO_2(e^-)|\text{-}Porph^{+\bullet}\text{-}Ru^{II}-OH_2^{2+}$. The methylene bridge linking the porphyrin chromophore and the carbene catalyst greatly decreases electronic coupling as shown by ground state UV−visible spectra with no evidence for electronic coupling. In spite of the large free energy change of ∼0.6 V for intra-assembly electron transfer, $SnO_2(e^-)|\text{-}Porph^{+\bullet}\text{-}Ru^{II}-OH_2^{2+} \rightarrow SnO_2(e^-)|\text{-}Porph\text{-}Ru^{III}-OH_2^{3+}$, back electron transfer is dominated by remote electron transfer to the electrode in $SnO_2(e^-)|\text{-}Porph\text{-}Ru^{III}-OH_2^{3+}$. There is clear evidence from related sensitizer−electron donor assemblies on the role of electron transfer distance on back electron transfer.[11]

As noted above, inclusion of the bridge increases the site-to-site electron transfer distance from the SnO_2 electrode to the acceptor by ∼8 Å. In prior studies on nanocrystalline SnO_2 as the semiconductor in dye sensitized solar cells (DSSCs), it has been shown that SnO_2 has a relatively low internal barrier toward intra-assembly electron transfer compared to other common wide band gap semiconductors. On TiO_2, back electron transfer is dictated by electrode dynamics and the interconversion between the internal and surface states at the electrode.[33] The data obtained here, with $k_{cr} = 1.0\ (\pm 0.3) \times 10^7\ s^{-1}$ for the rapid porphyrin-based reaction, over an electron transfer distance of ∼10 Å, provide a direct measure of the rate constant for back electron transfer from the electrode to the oxidized porphyrin. Remote back electron transfer from the remote Ru(III) catalyst to the electrode occurs with $k'_{cr} = 2.5\ (\pm 0.4) \times 10^4\ s^{-1}$ over an average electron transfer distance of ∼18 Å.

CONCLUSION

In this study, we have synthesized a covalently linked chromophore−catalyst assembly with a high oxidation potential porphyrin as chromophore in a surface-bound assembly with the addition of a chemically linked form of the water oxidation catalyst $[Ru(tpy)(bim\text{-}py)(OH_2)]^{2+}$. The results of transient absorption measurements on the porphyrin on SnO_2 at pH 4.7 show that in the assembly, $SnO_2|\text{-}Porph\text{-}Ru^{II}-OH_2^{2+}$, rapid, quantitative electron injection occurs from the porphyrin excited state into the SnO_2 conduction band. Injection is followed by competing events with ∼1/2 of the oxidative equivalents reaching the outside of the films to give the remote redox-separated state, $SnO_2(e^-)|\text{-}Porph\text{-}Ru^{III}-OH_2^{3+}$. Partial transfer of the injected oxidative equivalents occurs, apparently due to local transient medium effects that stabilize the intermediate bridged-based state, $SnO_2(e^-)|\text{-}Porph^{+\bullet}\text{-}Ru^{II}-OH_2^{2+}$.

The effect of selective trapping of the oxidative equivalent has provided a basis for investigating electron transfer from the electrode to the remote isomer, $SnO_2(e^-)|\text{-}Porph\text{-}Ru^{III}-OH_2^{3+}$, and from the internal isomer to the electrode, $SnO_2(e^-)|\text{-}Porph^{+\bullet}\text{-}Ru^{II}-OH_2^{2+}$. The rate constants are $k_{cr} = 1.0\ (\pm 0.3) \times 10^7\ s^{-1}$ for adjacent electron transfer from the electrode to oxidized porphyrin and significantly retarded $k'_{cr} = 2.5\ (\pm 0.4) \times 10^4\ s^{-1}$ for remote back electron transfer from the electrode to Ru(III). The latter reaction occurs over a distance of ∼18 Å by back electron transfer through the intervening porphyrin bridge.

ASSOCIATED CONTENT

Supporting Information

The Supporting Information is available free of charge on the ACS Publications website at DOI: 10.1021/acs.jpcc.7b11711.

NMR of assembly, cyclic voltammetry, and UV−vis of assembly on metal oxide surfaces, ns-TA of compound **2** (PDF)

AUTHOR INFORMATION

Corresponding Authors

*E-mail: tjmeyer@email.unc.edu.
*E-mail: gjmeyer@email.unc.edu.

ORCID

Ke Hu: 0000-0002-0240-7192
Gerald J. Meyer: 0000-0002-4227-6393
Thomas J. Meyer: 0000-0002-7006-2608

Author Contributions

†A.N. and K.H. contributed equally to this work.

Notes

The authors declare no competing financial interest.

ACKNOWLEDGMENTS

This research was funded solely by the UNC EFRC: Center for Solar Fuels, an Energy Frontier Research Center funded by the US Department of Energy, Office of Science, Office of Basic Energy Sciences, under Award DE-SC0001011

REFERENCES

(1) Concepcion, J. J; House, R. L; Papanikolas, J. M; Meyer, T. J. Chemical Approaches to Artificial Photosynthesis. *Proc. Natl. Acad. Sci. U. S. A.* **2012**, *109*, 15560−15564.
(2) Ashford, D. L.; Gish, M. K.; Vannucci, A. K.; Brennaman, M. K.; Templeton, J. L.; Papanikolas, J. M.; Meyer, T. J. Molecular

DOI: 10.1021/acs.jpcc.7b11711
J. Phys. Chem. C 2018, 122, 13455−13461

Chromophore−Catalyst Assemblies for Solar Fuel Applications. *Chem. Rev.* **2015**, *115*, 13006−13049.
(3) Brennaman, M. K.; Dillon, R. J.; Alibabaei, L.; Gish, M. K.; Dares, C. J.; Ashford, D. L.; House, R. L.; Meyer, G. J.; Papanikolas, J. M.; Meyer, T. J. Finding the Way to Solar Fuels with Dye-Sensitized Photoelectrosynthesis Cells. *J. Am. Chem. Soc.* **2016**, *138*, 13085−13102.
(4) Li, L.-L.; Diau, E. W.-G. Porphyrin-Sensitized Solar Cells. *Chem. Soc. Rev.* **2013**, *42*, 291−304.
(5) Mathew, S.; Yella, A.; Gao, P.; Humphry-Baker, R.; Curchod, B. F. E.; Ashari-Astani, N.; Tavernelli, I.; Rothlisberger, U.; Nazeeruddin, M. K.; Grätzel, M. Dye-Sensitized Solar Cells with 13% Efficiency Achieved through the Molecular Engineering of Porphyrin Sensitizers. *Nat. Chem.* **2014**, *6*, 242−247.
(6) Yamamoto, M.; Wang, L.; Li, F.; Fukushima, T.; Tanaka, K.; Sun, L.; Imahori, H. Visible Light-Driven Water Oxidation Using a Covalently-Linked Molecular Catalyst−sensitizer Dyad Assembled on a TiO 2 Electrode. *Chem. Sci.* **2016**, *7*, 1430−1439.
(7) Nayak, A.; Knauf, R. R.; Hanson, K.; Alibabaei, L.; Concepcion, J. J.; Ashford, D. L.; Dempsey, J. L.; Meyer, T. J. Synthesis and Photophysical Characterization of Porphyrin and porphyrin−Ru(ii) Polypyridyl Chromophore−catalyst Assemblies on Mesoporous Metal Oxides. *Chem. Sci.* **2014**, *5*, 3115−3119.
(8) Moore, G. F.; Blakemore, J. D.; Milot, R. L.; Hull, J. F.; Song, H.; Cai, L.; Schmuttenmaer, C. A.; Crabtree, R. H.; Brudvig, G. W. A Visible Light Water-Splitting Cell with a Photoanode Formed by Codeposition of a High-Potential Porphyrin and an Iridium Water-Oxidation Catalyst. *Energy Environ. Sci.* **2011**, *4*, 2389−2392.
(9) Concepcion, J. J.; Jurss, J. W.; Norris, M. R.; Chen, Z.; Templeton, J. L.; Meyer, T. J. Catalytic Water Oxidation by Single-Site Ruthenium Catalysts. *Inorg. Chem.* **2010**, *49*, 1277−1279.
(10) Nayak, A.; Roy, S.; Sherman, B. D.; Alibabaei, L.; Lapides, A. M.; Brennaman, M. K.; Wee, K. R.; Meyer, T. J. Phosphonate-Derivatized Porphyrins for Photoelectrochemical Applications. *ACS Appl. Mater. Interfaces* **2016**, *8*, 3853−3860.
(11) Hu, K.; Blair, A. D.; Piechota, E. J.; Schauer, P. A.; Sampaio, R. N.; Parlane, F. G. L.; Meyer, G. J.; Berlinguette, C. P. Kinetic Pathway for Interfacial Electron Transfer from a Semiconductor to a Molecule. *Nat. Chem.* **2016**, *8*, 853−859.
(12) Laha, J. K.; Dhanalekshmi, S.; Taniguchi, M.; Ambroise, A.; Lindsey, J. S. A Scalable Synthesis of Meso-Substituted Dipyrromethanes. *Org. Process Res. Dev.* **2003**, *7*, 799−812.
(13) Wen, L.; Li, M.; Schlenoff, J. B. Polyporphyrin Thin Films from the Interfacial Polymerization of Mercaptoporphyrins. *J. Am. Chem. Soc.* **1997**, *119*, 7726−7733.
(14) Muthukumaran, K.; Loewe, R. S.; Ambroise, A.; Tamaru, S.; Li, Q.; Mathur, G.; Bocian, D. F.; Misra, V.; Lindsey, J. S. Porphyrins Bearing Arylphosphonic Acid Tethers for Attachment to Oxide Surfaces. *J. Org. Chem.* **2004**, *69*, 1444−1452.
(15) Alakonda, L.; Periasamy, M. Simple and Convenient Methods for N-Arylation of Heterocycles and Diphenylamine. *Synthesis* **2012**, *44*, 1063−1068.
(16) Alibabaei, L.; Farnum, B. H.; Kalanyan, B.; Brennaman, M. K.; Losego, M. D.; Parsons, G. N.; Meyer, T. J. Atomic Layer Deposition of TiO2 on Mesoporous nanoITO: Conductive Core-Shell Photoanodes for Dye-Sensitized Solar Cells. *Nano Lett.* **2014**, *14*, 3255−3261.
(17) Alibabaei, L.; Brennaman, M. K.; Norris, M. R.; Kalanyan, B.; Song, W.; Losego, M. D.; Concepcion, J. J.; Binstead, R. a.; Parsons, G. N.; Meyer, T. J. Solar Water Splitting in a Molecular Photoelectrochemical Cell. *Proc. Natl. Acad. Sci. U. S. A.* **2013**, *110*, 20008−20013.
(18) Alibabaei, L.; Sherman, B. D.; Norris, M. R.; Brennaman, M. K.; Meyer, T. J. Visible Photoelectrochemical Water Splitting into H_2 and O_2 in a Dye-Sensitized Photoelectrosynthesis Cell. *Proc. Natl. Acad. Sci. U. S. A.* **2015**, *112*, 5899−5902.
(19) Hanson, K.; Brennaman, M. K.; Ito, A.; Luo, H.; Song, W.; Parker, K. A.; Ghosh, R.; Norris, M. R.; Glasson, C. R. K.; Concepcion, J. J.; et al. Structure−Property Relationships in Phosphonate-Derivatized, Ru II Polypyridyl Dyes on Metal Oxide Surfaces in an Aqueous Environment. *J. Phys. Chem. C* **2012**, *116*, 14837−14847.
(20) Brennan, B. J.; Portolés, M. J. L.; Liddell, P. A.; Moore, T. A.; Moore, A. L.; Gust, D. Comparison of Silatrane, Phosphonic Acid, and Carboxylic Acid Functional Groups for Attachment of Porphyrin Sensitizers to TiO 2 in Photoelectrochemical Cells. *Phys. Chem. Chem. Phys.* **2013**, *15*, 16605−16614.
(21) Norris, M. R.; Concepcion, J. J.; Harrison, D. P.; Binstead, R. A.; Ashford, D. L.; Fang, Z.; Templeton, J. L.; Meyer, T. J. Redox Mediator Effect on Water Oxidation in a Ruthenium-Based Chromophore-Catalyst Assembly. *J. Am. Chem. Soc.* **2013**, *135*, 2080−2083.
(22) Rodriguez, J.; Kirmaier, C.; Holten, D. Optical Properties of Metalloporphyrin Excited States. *J. Am. Chem. Soc.* **1989**, *111*, 6500−6506.
(23) Watson, D. F.; Marton, A.; Stux, A. M.; Meyer, G. J. Influence of Surface Protonation on the Sensitization Efficiency of Porphyrin-Derivatized TiO2. *J. Phys. Chem. B* **2004**, *108*, 11680−11688.
(24) Williams, G.; Watts, D. C. Non-Symmetrical Dielectric Relaxation Behaviour Arising from a Simple Empirical Decay Function. *Trans. Faraday Soc.* **1970**, *66*, 80−85.
(25) Lindsey, C. P.; Patterson, G. D. Detailed Comparison of the Williams−Watts and Cole−Davidson Functions. *J. Chem. Phys.* **1980**, *73*, 3348−3357.
(26) Ward, C. L.; O'Donnell, R. M.; DiMarco, B. N.; Meyer, G. J. Kinetic Resolution of Charge Recombination and Electric Fields at the Sensitized TiO2 Interface. *J. Phys. Chem. C* **2015**, *119*, 25273−25281.
(27) Morseth, Z. A.; Wang, L.; Puodziukynaite, E.; Leem, G.; Gilligan, A. T.; Meyer, T. J.; Schanze, K. S.; Reynolds, J. R.; Papanikolas, J. M. Ultrafast Dynamics in Multifunctional Ru(II)-Loaded Polymers for Solar Energy Conversion. *Acc. Chem. Res.* **2015**, *48*, 818−827.
(28) Ashford, D. L.; Song, W.; Concepcion, J. J.; Glasson, C. R. K.; Brennaman, M. K.; Norris, M. R.; Fang, Z.; Templeton, J. L.; Meyer, T. J. Photoinduced Electron Transfer in a Chromophore-Catalyst Assembly Anchored to TiO2. *J. Am. Chem. Soc.* **2012**, *134*, 19189−19198.
(29) Remsing, R. C.; McKendry, I. G.; Strongin, D. R.; Klein, M. L.; Zdilla, M. J. Frustrated Solvation Structures Can Enhance Electron Transfer Rates. *J. Phys. Chem. Lett.* **2015**, *6*, 4804−4808.
(30) Remsing, R. C.; Klein, M. L. Solvation Dynamics in Water Confined within Layered Manganese Dioxide. *Chem. Phys. Lett.* **2017**, *683*, 478−482.
(31) Kirner, S. V.; Guldi, D. M.; Megiatto, J. D.; Schuster, D. I. Synthesis and Photophysical Properties of New Catenated Electron Donor−acceptor Materials with Magnesium and Free Base Porphyrins as Donors and C60 as the Acceptor. *Nanoscale* **2015**, *7*, 1145−1160.
(32) Brennaman, M. K.; Norris, M. R.; Gish, M. K.; Binstead, R. A.; Brown, R. J.; Lapides, A. M.; Song, W.; Alibabaei, L.; Concepcion, J. J.; Templeton, J. L.; et al.. Injection and Cross-Surface Electron Transfer in a Ruthenium-Based Chromophore-Catalyst Assembly on TiO2. Manuscript in Preparation.
(33) Green, A. N. M.; Palomares, E.; Haque, S. A.; Kroon, J. M.; Durrant, J. R. Charge Transport versus Recombination in Dye-Sensitized Solar Cells Employing Nanocrystalline TiO2 and SnO2 Films. *J. Phys. Chem. B* **2005**, *109*, 12525−12533.

DOI: 10.1021/acs.jpcc.7b11711
J. Phys. Chem. C 2018, 122, 13455−13461